Journal of Sustainable Development of Energy, Water and Environment Systems

http://www.sdewes.org/jsdewes

Year 2021, Volume 9, Issue 1, 1080326

Entropy Analysis of Complete Condensation of Saturated Steam on a Vertical Wall Using Nusselt Velocity and Temperature Profile in a Condensate Layer

Martina Rauch*[1], Saša Mudrinić[2], Antun Galović[3]

[1]Department of Thermodynamics and Thermal and Process Engineering, University of Zagreb, Faculty of Mechanical Engineering and Naval Architecture, Ivana Lučića 5, 10000 Zagreb, Croatia
e-mail: martina.rauch@fsb.hr

[2]Department of Thermodynamics and Thermal and Process Engineering, University of Zagreb, Faculty of Mechanical Engineering and Naval Architecture, Ivana Lučića 5, 10000 Zagreb, Croatia
e-mail: sasa.mudrinic@fsb.hr

[3]Department of Thermodynamics and Thermal and Process Engineering, University of Zagreb, Faculty of Mechanical Engineering and Naval Architecture, Ivana Lučića 5, 10000 Zagreb, Croatia
e-mail: antun.galovic@fsb.hr

Cite as: Rauch, M., Mudrinić, S., Galović, A., Entropy Analysis of Complete Condensation of Saturated Steam on a Vertical Wall Using Nusselt Velocity and Temperature Profile in a Condensate Layer, J. sustain. dev. energy water environ. syst., 9(1), 1080326, 2021, DOI: https://doi.org/10.13044/j.sdewes.d8.0326

ABSTRACT

In this paper an analytical model for calculation of entropy production for Nusselt model of condensation of pure substance vapour is given. Model development starts from basic two-dimensional integral equation for entropy production and describes film condensation on a vertical wall. Model covers entropy production, which is a result of two-dimensional heat transfer in a condensate layer, existence of velocity gradient and condensate layer viscosity. Entropy contribution of each of the members is explicitly derived in a closed form and the results of calculation are shown in the appropriate diagrams. Diagrams present film condensation of dry saturated water steam and dry saturated ammonia steam, both with saturation temperature of 100 °C with surface wall temperature of 98.5 °C. Obtained equations and presentation of the related results have shown that dominant entropy production is directly connected only with heat conduction in y-axis direction, where y-axis corresponds with thickness of condensate layer.

KEYWORDS

Entropy analysis, Analytical model, Film condensation, Nusselt's theory.

INTRODUCTION

The theory of film condensation has been developed by Nusselt [1] in 1916. Presumptions in his model are laminar condensate outflow and constant physical properties of the condensate, vapour-liquid heat transfer is carried out only by condensation on a free surface and not with conduction on the steam side. Shear stress of the vapour-liquid on a free surface is ignored, as well as the momentum and advection heat transfer in a condensate layer. The result of those presumptions is a linear temperature profile in a condensate layer and velocity profile, which follows the principle of parabola.

* Corresponding author

Many authors presented different thermodynamic analysis and models in order to provide conclusions about the effect of condensation. Hygum *et al*. [2] developed model which is in a good agreement with the classical Nusselt equations for the laminar flow regime. Using the entropic lattice Boltzmann method extended with a free surface formulation of the evaporation-condensation problem, model for vapour condensation on vertical hydrophilic surfaces is developed. Li and Yang [3] performed thermodynamic analysis which presented the way the geometric parameter-ellipticity affects entropy generation during film-wise condensation heat transfer process. Reviewing the impact of viscous force, gravity and centrifugal force on condensation heat transfer, Wu *et al*. [4] elaborated a theoretical model. Elaborated model places emphasis on laminar flow for film condensation heat transfer of pure steam in the spiral coil tube. Wu *et al*. [5] also provided theoretical model of homogeneous flow to offer a solution for pure steam film condensation heat transfer of the shell side of the spiral coil. Charef *et al*. [6] directed their numerical study on the liquid film condensation from the vapour-gas mixtures inside a vertical tube. Within mentioned study an implicit finite difference method was used to give a solution to the equations for liquid film and gas flow. In order to examine the effects of vapour velocity and wall temperature on the condensate film thickness and heat flow rate in the laminar and wavy regimes, Lee and Son [7] performed numerical simulation of film condensation in a vertical downward channel flow by employing the sharp-interface level-set method. Also, an analytical model for the internal film condensation by including the effect of vapour flow in the Nusselt model was developed. In order to include the effects of interfacial slip, Pati *et al*. [8] extended Nusselt's theory on film condensation over vertical surfaces and brought enhancement in Nusselt number as a consequence of an effective interfacial slip as compared to that in case of without slip. Ali *et al*. [9] numerically simulated the fluid flow and the turbulent/laminar water heat transfer through the annulus side of the conically tube. Two correlations were proposed for the prediction of the friction factor and the Nusselt number. Yang *et al*. [10] focused on the thermodynamic analysis of saturated vapour flowing slowly onto and condensing on an elliptical tube with variable wall temperature, Qu *et al*. [11] presented a numerical solution for film condensation on a vertical plate sintered with metallic foam.

Many scientific papers presented experimental data on condensation of steam. Wu *et al*. [12] performed numerical simulation and performance comparison to establish the Spiral Wound Heat Exchanger (SWHE) partial geometric models with various tube diameters, pitches and spacing bar thickness. Ahn *et al*. [13] conducted an experiment on condensation heat transfer to develop a condensation model considering the structure of separated flow patterns. Also, Rajkumar *et al*. [14] presented experimental data on the condensation of steam on vertical bare copper tubes and lead coated copper tubes. In Yan *et al*. [15] research, comparing the simulation results (condensation section calculation) and the experimental values show that the simulated results are consistent with the experimental value and can predict the performance of the naphthalene heat pipe.

Through a review of the papers it is possible to see overview of different studies regarding entropy analysis. Some studies [16] use the entropy generation minimization method to optimize a saturated vapour flowing slowly onto and condensed on an isothermal horizontal tube. Esfahani and Modirkhazeni [17] analyse the entropy generation number in forced convection film condensation on a horizontal isothermal elliptical tube. On the other hand, some studies [18] are focused on entropy generation and exergy destruction of condensing steam flow in turbine blade with roughness. Entropy generation and exergy loss of nanofluid refrigerant condensation is experimentally examined in Sheikholeslami *et al*. [19]. The results showed that with the increase of concentration of nanoparticles, the frictional entropy generation also increases. However, thermal entropy generation decreases with the increase of vapour quality, mass fraction of nanoparticles and mass flux.

Numerous studies numerically simulated heat transfer processes, especially process of condensation with emphasis on entropy analysis. Natural convective heat transfer and entropy generation of alumina/water nano-fluid in an inclined enclosure under the magnetic field was examined in Aghakhani *et al*. [20]. Heat transfer rate and entropy generation increases 2.69 and 3.77 times, respectively, by increasing the Rayleigh number, while they decrease with the increase of Hartmann number. Gholamalipour *et al*. [21] present impact of the horizontal and vertical eccentricity of the heat source for different values of Darcy and Rayleigh numbers on the entropy generation of natural convection flow of nanofluid. For low values of Darcy and Rayleigh number, entropy generation is highly affected by the increase of eccentricity. Volume of fluid model is used in Rashidi *et al*. [22] to investigate possibilities for improvement of a single slope solar still productivity and to simulate the condensation and evaporation in the solar still. Moreover, entropy analysis was also performed and the results showed that the maximum values of thermal and viscous entropy generation are located around the top and the bottom surface of the solar still. Aliabadi *et al*. [23] investigated the effect of water nano-droplets in saturated steam flow. The results showed that temperature, pressure, mass fraction of liquid and entropy increases with the increase in number of water droplets at the nozzle inlet. Vatanmakan *et al*. [24] presented numerical analysis of volumetric heating impact on condensing steam flow in the stationary cascade of turbine blades. Entropy generation increases with the increase of volumetric heating, but when liquid phase disappears, the entropy generation shows a descending trend.

Many of the scientific papers and books which deal with entropy analysis of Nusselt's film condensation conclude that generated, almost overall, entropy is a result of existence of the temperature gradient trending towards the thickness of condensate layer, but those papers do not present the explicit mathematical proof for that claim. Basic idea and motive for this paper is obtaining the explicit amount of entropy contribution of all members in overall entropy generation and their subsequent comparison, with the aim to validate the claims of many researchers.

It can be confirmed, according to general Gouy-Stodola theorem [25], that overall entropy generation of an isolated system, which includes all relevant parameters of the observed process, directly effects the unwanted exergy destruction of valuable primary energy. This means that it is very important to conduct the processes in a way that they generate as less entropy as possible, thus consuming less valuable primary energy as well as producing less impact on the environment. Need for energy savings and environmental compartments protection during the thermal processes are one of the basic features of the energy-water nexus concept [26]. Since condensation process is significantly present in many heat facilities and it is therefore generating entropy, development of the entropy generation algorithm presented in this paper is of great importance. Based on the analysis of the obtained algorithm it can be concluded which significant parameters can be used to reduce the entropy generation. One of the main benefits of entropy generation decrease is the reduction of the heat load of an important natural resource – cooling water. This benefit is in accordance with sustainable development principles.

DEVELOPMENT OF THE MATHEMATICAL MODEL

An analytical mathematical model is derived for calculation of entropy production for Nusselt model of film condensation on the plane wall. Model covers entropy production which is a result of two-dimensional heat transfer in a condensate layer, existence of velocity gradient and condensate layer viscosity, as shown in the following chapters.

Analysis of the effect of temperature gradient

According to Nusselt [1], velocity and temperature profile in the condensate layer is:

$$v_x(y) = \frac{g(\rho_k - \rho_p)}{\eta_k}\delta^2(x)\left[\frac{y}{\delta(x)} - \frac{1}{2}\left(\frac{y}{\delta(x)}\right)\right] \quad (1)$$

Velocity $v_x(y)$ on $y = \delta(x)$ is also maximum velocity which equals:

$$v_x[y = \delta(x)] = v_{x,\text{maks}} = \frac{g(\rho_k - \rho_p)\delta^2(x)}{2\eta_k} \quad (2)$$

$$T(x,y) = T_s + \frac{T' - T_s}{\delta(x)}y \quad (3)$$

Eq. (1) and eq. (3) are valid within the interval:

$$0 \le x \le X \quad (4a)$$

$$0 \le y \le \delta(x) \quad (4b)$$

According to Nusselt [1], thickness of the resulted condensate layer is calculated using the following equation:

$$\delta(x) = \left[\frac{4\eta_k\lambda_k(T' - T_s)x}{gr(\rho_k - \rho_p)\rho_k}\right]^{\frac{1}{4}} = Cx^{\frac{1}{4}} \quad (5a)$$

where constant (C) has a form:

$$C = \left[\frac{4\eta_k\lambda_k(T' - T_s)}{gr(\rho_k - \rho_p)\rho_k}\right]^{\frac{1}{4}} \quad (5b)$$

Eq. (1) to eq. (4) is valid as long as there is laminar condensate outflow along the vertical plane wall. According to Bejan [25], criterion which has to be fulfilled, for the case above is:

$$Re_{\delta(x)} = \frac{\bar{v}_X\delta(X)\rho_k}{\eta_k} < 30 \quad (6)$$

where velocity $\bar{v}_X$ can be calculated from mass flow rate of condensate reduced to wall width (b):

$$\frac{q_m}{b} = \frac{\alpha_m(T' - T_s)X}{r} \quad (7)$$

On the other side, amount of value q_m/b is gained from equation:

$$\Phi_L = \alpha_m(T' - T_s)X = \frac{q_m}{b}r \quad (8)$$

By inserting eq. (6) into eq. (8) followed by integration the requested value q_m/b is obtained:

$$\frac{q_{\mathrm{m}}}{b} = \frac{\alpha_{\mathrm{m}}(T' - T_{\mathrm{s}})X}{r} \tag{9}$$

Average convective heat transfer coefficient on a plane wall with given X is calculated according to Nusselt [1]:

$$\alpha_{\mathrm{m}} = \frac{4}{3}\sqrt[4]{\left[\frac{\rho_{\mathrm{k}}(\rho_{\mathrm{k}} - \rho_{\mathrm{p}})gr\lambda_{\mathrm{k}}^3}{4\eta_{\mathrm{k}}(T' - T_{\mathrm{s}})X}\right]} \tag{10}$$

From eq. (9), eq. (7) and eq. (5), velocity $[\bar{v}_{(X)}]$ is defined:

$$\bar{v}_X = \frac{\alpha_{\mathrm{m}}(T' - T_{\mathrm{s}})X}{\rho_{\mathrm{k}} r \delta(X)} \tag{11}$$

and using eq. (6), value of Nusselt number is checked, i.e., fulfilment of criteria given in eq. (6) is controlled.

Entropy production in convective heat transfer is a result of heat conduction and dissipation of mechanical energy. Their determination is relatively simple with presumed laminar condensate flow. In such laminar flow, both forms of entropy production rest on molecular level through values of thermal conductivity (λ_{k}) as well as dynamic viscosity (η_{k}), with existence of temperature gradients and velocity gradients. Based on that, the expression for local entropy production is Cengel [27]:

$$S_{\mathrm{cond}} = \frac{\lambda_{\mathrm{k}}}{T^2}\left[\left(\frac{\partial T}{\partial x}\right)^2 + \left(\frac{\partial T}{\partial y}\right)^2\right] \tag{12}$$

$$S_{\mathrm{dis}} = \frac{\eta_{\mathrm{k}}}{T}\left\{2\left[\left(\frac{\partial v_x}{\partial x}\right)^2 + \left(\frac{\partial v_y}{\partial y}\right)^2\right] + \left(\frac{\partial v_x}{\partial y} + \frac{\partial v_y}{\partial x}\right)^2\right\} \tag{13}$$

Using differential equations above, generated entropy expressed in W/mK can be expressed with the following integral equation:

$$\dot{S}_{\mathrm{gen}} = \int_0^X \int_0^{\delta(x)} \frac{\lambda_{\mathrm{k}}}{T^2}\left[\left(\frac{\partial T}{\partial x}\right)^2 + \left(\frac{\partial T}{\partial y}\right)^2\right] dxdy + \int_0^X \int_0^{\delta(x)} \frac{\eta_{\mathrm{k}}}{T}\left\{2\left[\left(\frac{\partial v_x}{\partial x}\right)^2 + \left(\frac{\partial v_y}{\partial y}\right)^2\right] + \left(\frac{\partial v_x}{\partial y} + \frac{\partial v_y}{\partial x}\right)^2\right\} dxdy \tag{14}$$

Where partial derivatives of temperature with respect to x and y coordinates stand for:

$$\left(\frac{\partial T}{\partial x}\right) = -\frac{T' - T_{\mathrm{s}}}{4C} y x^{-\frac{5}{4}} \tag{15a}$$

$$\left(\frac{\partial T}{\partial y}\right) = \frac{T' - T_{\mathrm{s}}}{\delta(x)} \tag{15b}$$

In observed case, the dominant temperature gradient is in y-axis direction, so in the first approximation, entropy generation for only existence of that temperature gradient is observed, which means that entropy contribution of other members in eq. (14) is ignored. So, using eq. (3) and boundary conditions in eq. (4a), eq. (4b) and eq. (14), the following equation is obtained:

$$\dot{S}_{\mathrm{gen,d}T/\mathrm{d}y} = \lambda_{\mathrm{k}}\left[\frac{T' - T_{\mathrm{s}}}{\delta(x)}\right]^2 \int_0^X dx \int_0^{\delta(x)} \frac{dy}{\left[T_{\mathrm{s}} + \frac{T' - T_{\mathrm{s}}}{\delta(x)} y\right]^2} \tag{16a}$$

Solution for second integral is obtained by importing the substitution:

$$u = T_s + \frac{T' - T_s}{\delta(x)} y \;\rightarrow\; y = \frac{(u - T_s)\delta(x)}{T' - T_s};\; \mathrm{d}y = \frac{\delta(x)}{T' - T_s} du \tag{a}$$

and crossing to variable (u) according to eq. (a), limits of integration are now:

$$y = 0; \qquad u = T_s \tag{b}$$

$$y = \delta(x); \qquad u = T' \tag{c}$$

With imported values eq. (14) has a form:

$$\dot{S}_{\mathrm{gen},\mathrm{d}T/\mathrm{d}y} = \lambda_k \left(\frac{T' - T_s}{\delta(x)}\right)^2 \frac{\delta(x)}{T' - T_s} \int_0^X dx \int_{T_s}^{T'} \frac{du}{u^2} = \frac{\lambda_k (T' - T_s)^2}{T_s T'} \int_0^X \frac{dx}{\delta(x)} \tag{16b}$$

Upon conducted integration it is easy to come to the final expression for entropy generation:

$$\dot{S}_{\mathrm{gen},\mathrm{d}T/\mathrm{d}y} = \frac{4}{3} \frac{(T' - T_s)^2}{T' T_s} \left[\frac{gr(\rho_k - \rho_p)\rho_k \lambda_k^3 X^3}{4\eta_k (T' - T_s)}\right]^{\frac{1}{4}} \tag{16c}$$

The following operation shows the quantitative effect of the temperature gradient in x-axis direction $\partial T/\partial x$ (as a result of heat conduction) to entropy generation:

$$\dot{S}_{\mathrm{gen},\mathrm{d}T/\mathrm{d}x} = \int_0^X \int_0^{\delta(x)} \frac{\lambda_k}{T^2} \left[\left(\frac{\partial T}{\partial x}\right)^2\right] dx dy \tag{17a}$$

By inserting eq. (3) and eq. (15), and boundary conditions into eq. (17a), as well as substituting with eq. (a-c), the following form of the integral is obtained:

$$\dot{S}_{\mathrm{gen},\mathrm{d}T/\mathrm{d}x} = \frac{\lambda_k (T' - T_s)}{16 C^2} \int_0^X \delta(x) x^{-\frac{5}{2}} \int_{T_s}^{T'} \frac{\delta^2(x)(u^2 - 2T_s u + T_s^2)}{u^2} du dx \tag{17b}$$

By returning eq. (5) into eq. (17b), the final expression for entropy generation related to conductive (molecular) heat transfer in x-axis direction is:

$$\dot{S}_{\mathrm{gen},\mathrm{d}T/\mathrm{d}x} = \frac{1}{4} \left[\frac{\eta_k \lambda_k^5 (T' - T_s)^5 X}{gr(\rho_k - \rho_p)\rho_k}\right]^{\frac{1}{4}} \frac{(T')^2 - (T_s)^2 - 2T_s T' \ln \frac{T'}{T_s}}{T'} \tag{17c}$$

Overall entropy generation, due to existence of temperature gradients, in both y-axis and x-axis directions, equals sum of eq. (16c) and eq. (17c), i.e.:

$$\dot{S}_{\mathrm{gen,cond}} = \frac{4}{3} \frac{(T' - T_s)^2}{T' T_s} \left[\frac{gr(\rho_k - \rho_p)\rho_k \lambda_k^3 X^3}{4\eta_k (T' - T_s)}\right]^{\frac{1}{4}} + \frac{1}{4} \left[\frac{\eta_k \lambda_k^5 (T' - T_s)^5 X}{gr(\rho_k - \rho_p)\rho_k}\right]^{\frac{1}{4}} \frac{(T')^2 - (T_s)^2 - 2T_s T' \ln \frac{T'}{T_s}}{T'} \tag{18}$$

The dominant temperature gradient ($\partial T/\partial y$) is in y-axis direction, which means that the entropy generation will be dominant due to that gradient, i.e., portion of entropy

generation caused by existence of gradient ($\partial T/\partial x$) will be irrelevant, what is confirmed by the results of the calculation.

Analysis of the effect of viscosity and velocity gradients to the amount of entropy generation

According to Nusselt [1], velocity profile $v_x(x, y)$ in a condensate layer has a form:

$$v_x(x,y) = \frac{g\left(\rho_\mathrm{k} - \rho_\mathrm{p}\right)}{\eta_\mathrm{k}}\left[\delta(x)y - \frac{1}{2}y^2\right] \tag{19}$$

and therefore, along with eq. (5), scalar value of velocity gradient (v_x) in x-axis direction follows:

$$\frac{\partial v_x}{\partial x} = \frac{1}{4}\frac{g\left(\rho_\mathrm{k} - \rho_\mathrm{p}\right)}{\eta_\mathrm{k}} C y x^{-\frac{3}{4}} \tag{20}$$

From the continuity equation:

$$\frac{\partial v_x}{\partial x} + \frac{\partial v_y}{\partial y} = 0 \tag{21}$$

follows the expression for scalar value of velocity gradient (v_y) in y-axis direction:

$$\frac{\partial v_y}{\partial y} = -\frac{1}{4}\frac{g\left(\rho_\mathrm{k} - \rho_\mathrm{p}\right)}{\eta_\mathrm{k}} C y x^{-\frac{3}{4}} \tag{22}$$

By integrating the equation above along y-axis and using the condition $v_y(x, y) = 0$, for $y = 0$, the expression for velocity $v_y(x, y)$ is obtained:

$$v_y(x,y) = -\frac{1}{8}\frac{g\left(\rho_\mathrm{k} - \rho_\mathrm{p}\right)}{\eta_\mathrm{k}} y^2 x^{-\frac{3}{4}} \tag{23}$$

From eq. (19) and eq. (23) follows:

$$\frac{\partial v_x}{\partial y} = \frac{g\left(\rho_\mathrm{k} - \rho_\mathrm{p}\right)}{\eta_\mathrm{k}}(\delta - y) \tag{24}$$

$$\frac{\partial v_y}{\partial x} = \frac{3}{32}\frac{g\left(\rho_\mathrm{k} - \rho_\mathrm{p}\right)}{\eta_\mathrm{k}} y^2 x^{-\frac{7}{4}} \tag{25}$$

Effect of η_k and value $(\partial v_x/\partial x)^2 + (\partial v_y/\partial y)^2$. By using eq. (3), eq. (5), eq. (20), eq. (22) and the second addend of eq. (14):

$$\dot{S}_\mathrm{gen} = \int_0^X \int_0^{\delta(x)} \frac{\eta_\mathrm{k}}{T}\left\{2\left[\left(\frac{\partial v_x}{\partial x}\right)^2 + \left(\frac{\partial v_y}{\partial y}\right)^2\right]\right\} dx dy \tag{26a}$$

The following expression for entropy generation is gained:

$$\dot{S}_{\mathrm{gen},\left[(\partial v_x/\partial x)^2 + (\partial v_y/\partial y)^2\right]} = \frac{g^2\left(\rho_\mathrm{k} - \rho_\mathrm{p}\right)^2}{\eta_\mathrm{k}^2} C^2 \int_0^H x^{-\frac{3}{2}} dx \int_0^{\delta(x)} \frac{y^2 dy}{\left[T_\mathrm{s} + \frac{T' - T_\mathrm{s}}{\delta(x)}\right]^2} \tag{26b}$$

By using substitution and boundary conditions from eq. (a-c), the expression above [eq. (26b)] is transformed into:

$$\dot{S}_{\text{gen},[(\partial v_x/\partial x)^2+(\partial v_y/\partial y)^2]} = \frac{g^2\left(\rho_\text{k}-\rho_\text{p}\right)^2}{\eta_\text{k}^2} C^5 \frac{1}{(T'-T_\text{s})^3}\left[u - 2T_\text{s}\ln u + T_\text{s}^2\left(-\frac{1}{u}\right)\right]_{T_\text{s}}^{T'} \int_0^H x^{-\frac{3}{4}} dx \quad (26c)$$

Therefore, the final solution of the eq. (26c) is:

$$\dot{S}_{\text{gen},[(\partial v_x/\partial x)^2+(\partial v_y/\partial y)^2]} = 2\sqrt{2}\left[\frac{g\eta_\text{k}\left(\rho_\text{k}-\rho_\text{p}\right)^3\lambda_\text{k}^5 X}{r^5\rho_\text{k}(T'-T_\text{s})^7}\right]^{\frac{1}{4}} \frac{(T')^2 - T_\text{s}^2 - 2T'T_\text{s}\ln\frac{T'}{T_\text{s}}}{T'} \quad (26d)$$

Effect of η_k and value $(\partial v_x/\partial y)^2$. Starting position for resolution of values above is again eq. (3), eq. (5), eq. (24) and part of eq. (14) with the following form:

$$\dot{S}_\text{gen} = \int_0^X \int_0^{\delta(x)} \frac{\eta_\text{k}}{T}\left(\frac{\partial v_x}{\partial y}\right)^2 dxdy \quad (27a)$$

By importing mentioned equations into eq. (27a):

$$\dot{S}_{\text{gen},(\partial v_x/\partial y)^2} = \eta_k \frac{g^2\left(\rho_\text{k}-\rho_\text{p}\right)^2}{\eta_\text{k}^2}\int_0^X dx \int_0^{\delta(x)} \frac{[(\delta(x)-y)]^2}{T_\text{s}+\frac{T'-T_\text{s}}{\delta(x)}y} dy \quad (27b)$$

Using the same substitution as well as the same boundary conditions, eq. (a-c), slightly longer integration leads to the final form of the eq. (27b):

$$\dot{S}_{\text{gen},(\partial v_x/\partial y)^2} = \frac{4}{7}H\left\{\frac{\left[g\left(\rho_\text{k}-\rho_\text{p}\right)\rho_\text{k}\right]^{\frac{5}{3}}4\eta_\text{k}\lambda_\text{k}X}{r_\text{k}(T'-T_\text{s})^{\frac{1}{3}}}\right\}^{\frac{3}{4}}\left[\begin{array}{l}\ln\frac{T'}{T_\text{s}} - 2\frac{T'-T-T_\text{s}\ln\frac{T'}{T_\text{s}}}{T'-T_\text{s}} + \\ \frac{(T')^2 - T_\text{s}^2 - 4T_\text{s}(T'-T_\text{s}) + 2T_\text{s}^2\ln\frac{T'}{T_\text{s}}}{2(T'-T_\text{s})^2}\end{array}\right] \quad (27c)$$

Effect of η_k and value $(\partial v_y/\partial x)^2$. Starting position for determining the effect of this gradient is eq. (3), eq. (5), eq. (25) and part of eq. (14):

$$\dot{S}_{\text{gen},(\partial v_y/\partial x)^2} = \int_0^X \int_0^{\delta(x)} \frac{\eta_\text{k}}{T}\left(\frac{\partial v_y}{\partial x}\right)^2 dxdy = \eta_\text{k}\int_0^X dx \int_0^{\delta(x)} \frac{\left(3g\frac{\rho_\text{k}-\rho_\text{p}}{24\eta_\text{k}}\right)^2 y^4 x^{-\frac{7}{2}}}{T_\text{s}+\frac{T'-T_\text{s}}{\delta(x)}dy} \quad (28a)$$

The equation above is rearranged into:

$$\dot{S}_{\text{gen},(\partial v_y/\partial x)^2} = \eta_\text{k}\frac{9}{1{,}024}\frac{g^2(\rho_\text{k}-\rho_\text{p})^2}{\eta_\text{k}^2}\int_0^X x^{-\frac{7}{2}}dx\int_0^{\delta(x)}\frac{y^4}{T_\text{s}+\frac{T'-T_\text{s}}{\delta(x)}dy}dy \quad (28b)$$

By using the substitution with boundary conditions, [eq. (a-c)], the equation above is translated to:

$$\dot{S}_{\text{gen},(\partial v_y/\partial x)^2} = \eta_\text{k}\frac{9}{1{,}024}\frac{g^2(\rho_\text{k}-\rho_\text{p})^2}{\eta_\text{k}(T'-T_\text{s})^5}C^5\int_0^X x^{-\frac{9}{4}}dx\int_{T_\text{s}}^{T'}\frac{(u-T_\text{s})^4}{u}du \quad (28c)$$

Solution of the integral above can also be found analytically, so the final solution is:

$$\dot{S}_{\mathrm{gen},(\partial v_y/\partial x)^2} = \frac{3}{1{,}280}\left[15T_\mathrm{s}^3T' - 4(T'T_\mathrm{s})^2 + T_\mathrm{s}^4 - (T')^4 - T_\mathrm{s}^4\ln\frac{T'}{T_\mathrm{s}}\right]\left\{\frac{4\eta_\mathrm{k}\lambda_\mathrm{k}\left[g\left(\rho_\mathrm{k}-\rho_\mathrm{p}\right)\right]^{\frac{3}{5}}}{r\rho_\mathrm{k}(T'-T_\mathrm{s})^3X}\right\}^{\frac{5}{4}} \quad (28d)$$

Effect of η_k and value $2(\partial v_y/\partial x)\,(\partial v_x/\partial y)$. The starting equation with the following form can be written, using eq. (3), eq. (5), eq. (24), eq. (25) and part of the eq. (14):

$$\dot{S}_{\mathrm{gen},2(\partial v_y/\partial x)\,(\partial v_x/\partial y)} = \int_0^X\int_0^{\delta(x)}\frac{\eta_\mathrm{k}}{T}\left(2\frac{\partial v_y}{\partial x}\frac{\partial v_x}{\partial y}\right)dxdy = \frac{2\times3}{32}\eta_\mathrm{k}\frac{\left[g(\rho_\mathrm{k}-\rho_\mathrm{p})\right]^2}{\eta_\mathrm{k}^2}\int_0^X x^{-\frac{7}{4}}dx\int_0^{\delta(x)}\frac{(\delta-y)y^2}{T_\mathrm{s}+\frac{T'-T_\mathrm{s}}{\delta(x)}y}dy \quad (29a)$$

Importing substitution eq. (a-c) into eq. (29a) the equation is translated into the following form:

$$\dot{S}_{\mathrm{gen},2(\partial v_y/\partial x)\,(\partial v_x/\partial y)} = \frac{3}{16}\frac{\left[g(\rho_\mathrm{k}-\rho_\mathrm{p})\right]^2C^4}{\eta_\mathrm{k}(T'-T_\mathrm{s})^3}\left[\int_{T_\mathrm{s}}^{T'}\frac{(u-T_\mathrm{s})^2}{u}du - \frac{1}{T'-T_\mathrm{s}}\int_{T_\mathrm{s}}^{T'}\frac{(u-T_\mathrm{s})^3}{u}du\right] \quad (29b)$$

With conducted integration and with inserting the marked limits of integration, through somewhat longer operation, the final solution is obtained:

$$\dot{S}_{\mathrm{gen},2(\partial v_y/\partial x)\,(\partial v_x/\partial y)} = \frac{g(\rho_\mathrm{k}-\rho_\mathrm{p})X^{\frac{1}{4}}}{(T'-T_\mathrm{s})^3r\rho_\mathrm{k}}\left\{\begin{array}{l}(T'-T_\mathrm{s})\left[\dfrac{(T')^2-T_\mathrm{s}^2}{2}-2T_\mathrm{s}(T'-T_\mathrm{s})+T_\mathrm{s}^2\ln\dfrac{T'}{T_\mathrm{s}}\right]- \\ \left\{\dfrac{(T')^3-T_\mathrm{s}^3}{3}-\dfrac{3}{2}T_\mathrm{s}[(T')^2-T_\mathrm{s}^2]\right. \\ \left.+3T_\mathrm{s}^3(T'-T_\mathrm{s})-T_\mathrm{s}^3\ln\dfrac{T'}{T_\mathrm{s}}\right\}\end{array}\right\} \quad (29c)$$

Overall entropy generation determined with the effect of condensate viscosity and velocity gradients in a laminar condensate layer is achieved by addition of eq. (26-29), which, with eq. (18), give overall entropy generation in laminar condensation of dry saturated steam on a vertical plane wall.

DISPLAY AND INTERPRETATION OF CALCULATION RESULTS

Within the framework of the interpretation of the calculation results, the saturation temperature of the laminar condensation of dry saturated water vapour and dry saturated ammonia vapour is ϑ_s = 100 °C, with vertical wall temperature being ϑ_s = 98.5 °C.

Condensation of water vapour

According to the previously developed algorithm, the results of the calculation and their interpretation are shown in this section, so the diagram in Figure 1 displays the values of convective heat transfer coefficient, heat flow rate and thickness of the resulting condensate, with regard to the height of the plane wall (X).

It can be seen from Figure 1 that the thickness of the resulting condensate $\delta(x)$, which was calculated according to eq. (5), increases with the increase in wall height (X), as does the heat flow rate (Φ_L), which is calculated according to eq. (8). It is interesting to note that the observed case revolves around extremely small thicknesses of the resulting condensate, ranging in size from 0.02 to 0.073 mm. In contrast, there is a decrease in the average convective heat transfer coefficient, calculated according to eq. (10), with an increase in wall height X.

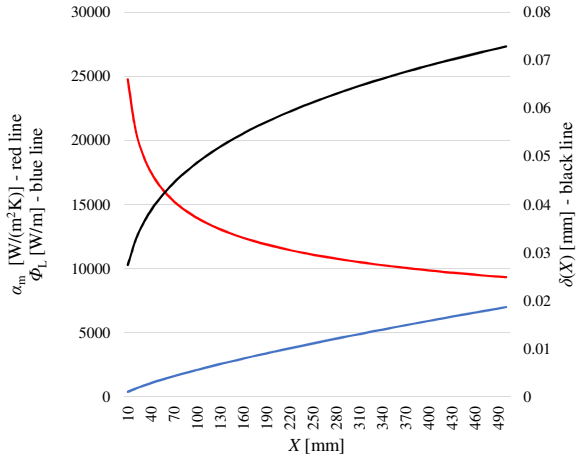

Figure 1. Dependence of heat transfer coefficient, heat flow rate and thickness of condensate film on the height of the plane wall X at total laminar condensation of saturated water steam with $\vartheta' = 100$ °C and $\vartheta_s = 98.5$ °C

It is important to observe both the local temperature profile and the local velocity profile in the resulting condensate film, whose values are determined by eq. (1) and eq. (3). Thus, the diagram in Figure 2 displays local values of temperatures $\vartheta[x, 0 \le y \le \delta(x)]$, as well as local values of velocities $v_x[X, 0 \le y \le \delta(x)]$ for the three selected plane wall heights $X = 100$, 300 and 500 mm. It can be seen that this is a linear profile of the temperatures in the condensate film with a maximum slope of the line corresponding to a wall height of 100 mm. It is evident that all lines pass through the same ordinate values of 98.5 °C and end with different $\delta(x)$ values at the ordinate value of 100 °C. The velocity profile in the condensate film $v_x[X, 0 \le y \le \delta(x)]$, for each selected wall height X has a square parabola profile and all the curves start from the origin and end with a local maximum at $y = \delta(x)$. It can be seen that the values of local velocities $v_x[X, 0 \le y \le \delta(x)]$ increase together with the increase in X. The local maximum values are determined by eq. (2). To conclude, the highest velocity gradients are on the wall, and they disappear at $y = \delta(x)$. The diagram also shows that only low condensate outflow rates appear in the observed case of laminar condensation of dry saturated water vapour, since it is evident that the values of maximum velocities range from 0.04 to 0.09 m/s.

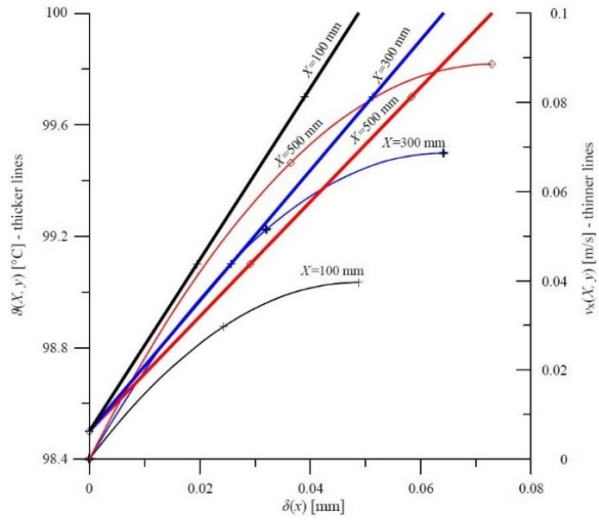

Figure 2. Dependence of local temperature $\vartheta[X, 0 \le y \le \delta(x)]$ and local velocity $v_x[X, 0 \le y \le \delta(x)]$ on local condensate thickness $\delta(y)$ and wall height $X = 100$, 300 and 500 mm for total laminar condensation of dry saturated water steam with $\vartheta' = 100$ °C and $\vartheta_s = 98.5$ °C

The bibliography offers various criteria that must be satisfied in order to induce laminar condensate outflow. For example, Cengel [27] specifies the criterion of $Re_{\delta(x)} \leq 10$, while in Bejan [25] the criterion is that $Re_{\delta(x)} \leq 30$. However, Bejan [25] states that there is laminar wave flow of the condensate within this region and that said criterion can also be subject to laminar flow. However, these two criteria specify substantially different plane wall heights against which laminar outflow of the condensate occurs, which is quantitatively depicted in the diagram in Figure 3. This diagram shows that, and this is physically justified, the criterion $Re_{\delta(x)} \leq 30$ provides for significantly greater wall heights X than the criterion $Re_{\delta(x)} \leq 10$. It can also be concluded that when it comes to wall height X, its surface temperature (ϑ_s) is also important. At lower wall temperatures, the sustainability of laminar condensate outflow involves very small wall heights. The diagram displays the results of the condensation of dry saturated water vapour with the pressure of 760 mm Hg, i.e., the corresponding saturation temperature $\vartheta' = 100$ °C. It is evident from the diagram that as the wall temperature reaches the saturation temperature, the wall height at which the laminar flow of the condensate is maintained markedly increases.

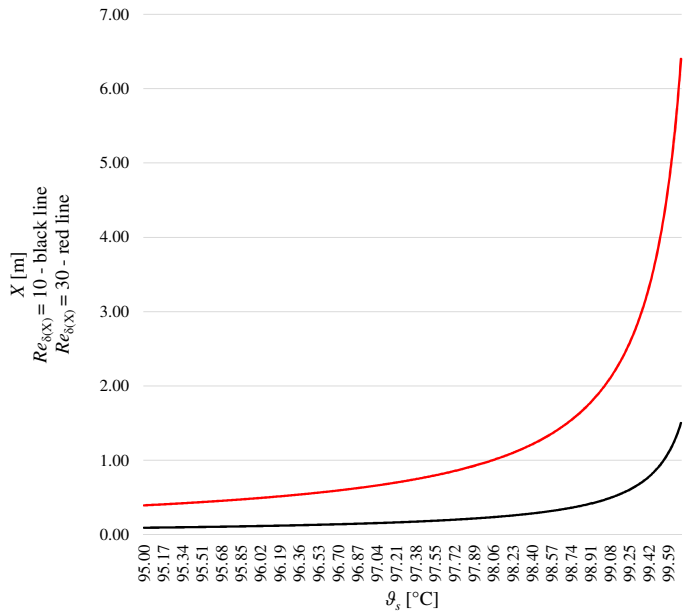

Figure 3. Dependence of wall height X on wall temperature ϑ_s and two different criterions for laminar condensate outflow with $\vartheta' = 100$ °C

Due to the aforementioned fact, the value of $\vartheta_s = 98.5$ °C was determined as the temperature at which the dry saturated water vapour with the temperature of 100 °C is condensed, and the following cases were calculated and analysed with regard to these conditions. Diagram in Figure 4 shows the dependence of the mass flow rate of the resulting condensate, reduced to a meter of plane wall width, depending on the wall height X. Both respective criteria $Re_{\delta(x)} \leq 10.0$, for which the value $X_{max} = 0.44$ m and $Re_{\delta(x)} \leq 30.0$, for which the value $X_{max} = 1.90$ m were included in the diagram. The diagram shows that the mass flow rate of the resulting condensate increases continuously with the increase of wall height X. It can also be concluded that small values of the mass flow rates are obtained.

The mass flow rate of the condensate is in direct relation, see eq. (7-11) with the thickness $\delta(x)$ of the resulting condensate, and therefore the diagram in Figure 5 shows the dependence of that thickness, represented by the black line, on the size X. In that same diagram, the red line represents the dependence of maximum velocity for free surface

flow of the condensate on the same wall height X. The velocity is calculated according to eq. (2). It can be seen that both variables continue to grow with the increase in the height wall X. In this case too, the value of size X varied up to 1.9 m, i.e., to the upper limit of the criterion $Re_{\delta(x)} \leq 30.0$.

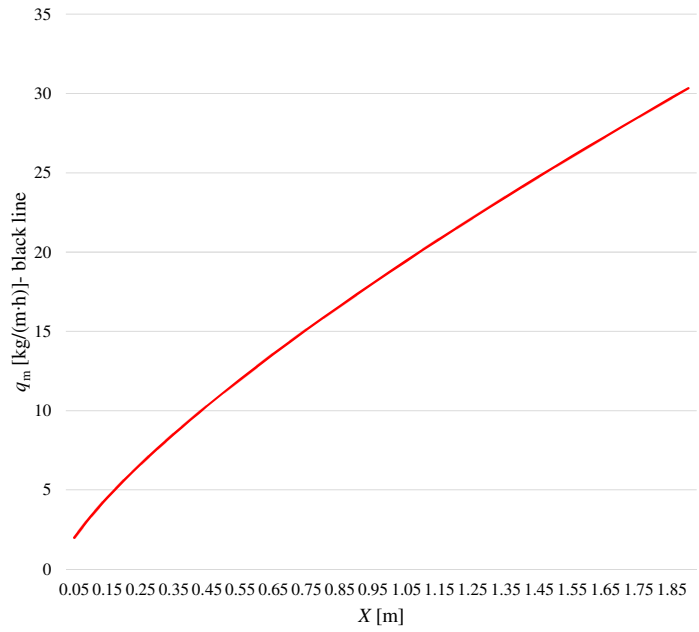

Figure 4. Dependence of mass flow rate on wall height X and two different criterions for laminar condensate outflow with ϑ' = 100 °C

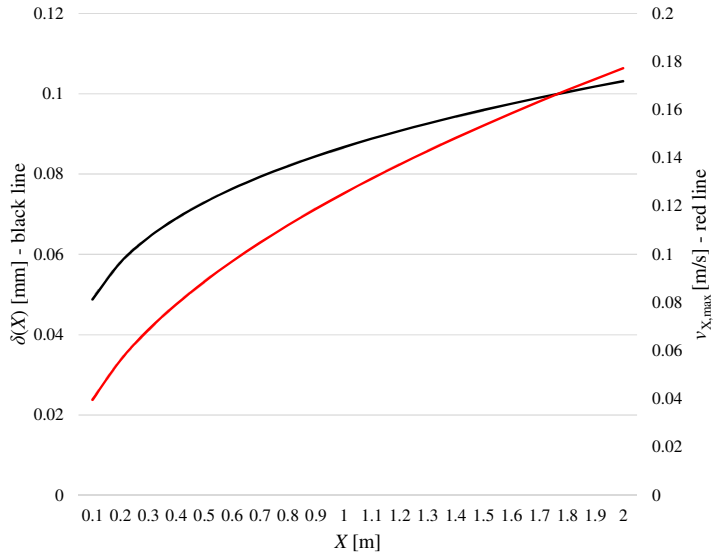

Figure 5. Dependence of thickness of condensate layer and maximum velocity on wall height X for laminar condensate outflow with ϑ_s = 98.5 °C and ϑ' = 100 °C

Figure 6 presents dependence of temperature gradients $\partial T/\partial y$ and $\partial T/\partial x$ on wall height X. It is clear that dominant temperature gradient is in y-axis direction ($\partial T/\partial y$), which means that the entropy generation will be dominant due to that gradient.

The diagrams presented so far have been related to the energy and mass results of the laminar film condensation calculation. However, since the motive of the paper primarily refers to entropy analysis, the following diagrams shall relate precisely to the representation of the entropy generation regarding the described occurrence.

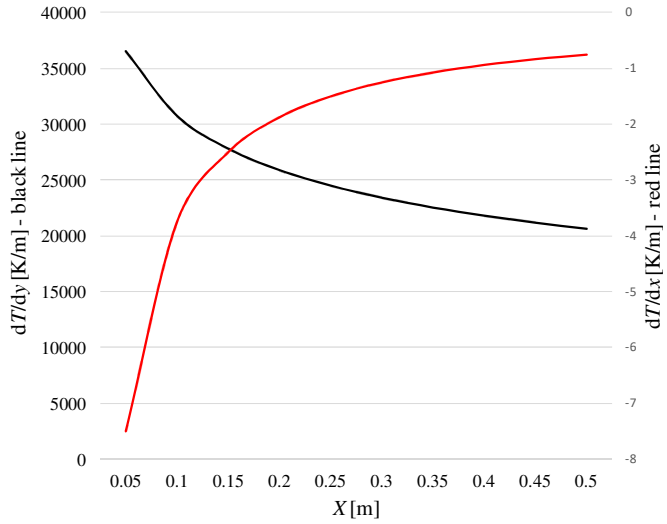

Figure 6. Dependence of temperature gradients $\partial T/\partial y$ and $\partial T/\partial x$ on wall height X for laminar condensate outflow

Accordingly, the diagram in Figure 7 shows the entropy generation considering the existence of temperature gradients in the directions of the y-axis and the x-axis, respectively, i.e., towards the starting eq. (14) and towards the ultimately derived eq. (18), in which the first addend represents entropy generation resulting from the temperature gradient in the direction of the y-axis, while the second addend represents the entropy generation from the existence of a temperature gradient in the direction of the x-axis.

The diagram shows that the dominant amount of entropy generation is a result of heat conduction in the direction of the y-axis, while the entropy generation resulting from heat conduction in the direction of the x-axis is practically imperceptible. This means that the entropy generation, due to the distinct temperature gradient in the direction of the y-axis, can be considered as the total entropy generation due to the conductive heat transfer in the condensate film. The second double integral in eq. (14) describes, as already mentioned, the entropy generation resulting from the influence of condensate viscosity and the velocity gradients existing therein.

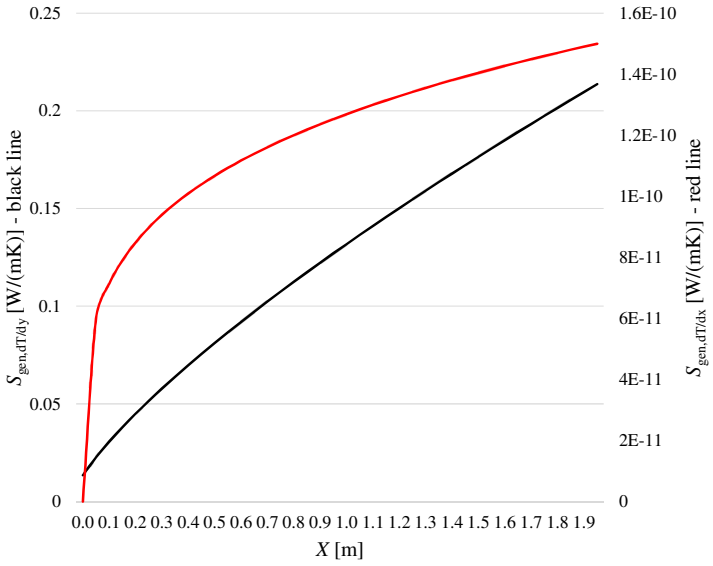

Figure 7. Dependence of entropy generation on wall height X and temperature gradients $\partial T/\partial y$ and $\partial T/\partial x$ with ϑ_s = 98.5 °C and ϑ' = 100 °C

The diagram in Figure 8 shows the entropy generation as a result of the viscosity and sum of squares of velocity gradients. The result of the calculation is given as a function of the height of the flat wall X, while maintaining the constant sizes described in Figure 8. The diagram shows that the value of this entropy generation is continuously growing with the increase of the wall height X, in such a way that the biggest increase occurs at the beginning of the formation of the laminar film of the condensate, and later this increase gets curtailed. However, the results of the calculations show that this part of the entropy generation is extremely small and has virtually no effect on the total entropy generation.

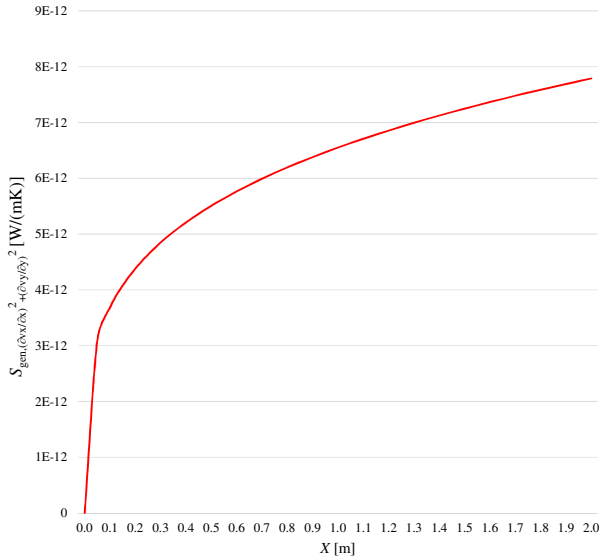

Figure 8. Dependence of entropy generation on wall height X and sum of squared velocity gradients $(\partial v_x/\partial x)^2 + (\partial v_y/\partial y)^2$ with $\eta_k = 282 \times 10^{-6}$ Pas, $\vartheta_s = 98.5$ °C and $\vartheta' = 100$ °C

The diagram in Figure 9 shows the entropy generation due to the viscosity of the condensate and the square of the velocity gradient $(\partial v_x/\partial y)^2$. The diagram shows that this entropy input also increases with the increasing of X, in such a way that this increase is bigger at higher values of X. These results also show that the absolute amount of entropy generation is barely noticeable, yet bigger than the one from the case shown in Figure 7 for 10^5 orders of magnitude. That is in fact in accordance with the physics of the problem, because the velocity gradient $\partial v_x/\partial y$ is by far the highest. Therefore, this entropy input has practically no meaning, so it can be ignored when calculating the total entropy balance.

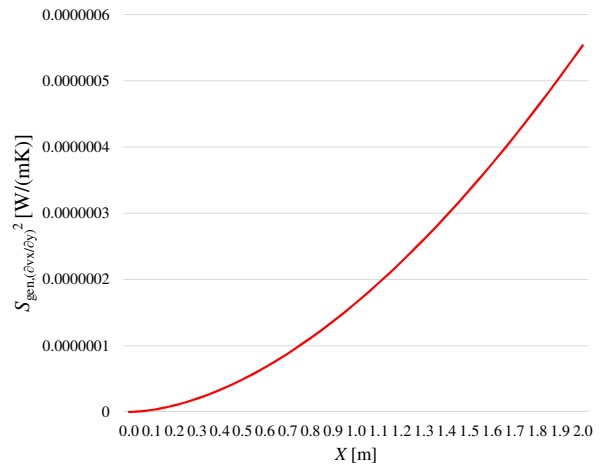

Figure 9. Dependence of entropy generation on wall height X and squared velocity gradient $(\partial v_x/\partial y)^2$ with $\eta_k = 282 \times 10^{-6}$ Pas, $\vartheta_s = 98.5$ °C and $\vartheta' = 100$ °C

Figure 10 shows the dependence of entropy production on the flat wall height X, the square of the velocity gradient $(\partial v_y/\partial x)^2$, and the viscosity of the condensate. This diagram also shows that this is also a very small, therefore irrelevant, entropy input. Its greatest value is at the formation of a laminar condensate film and upon reaching the wall height of 0.4 m it gets to zero value.

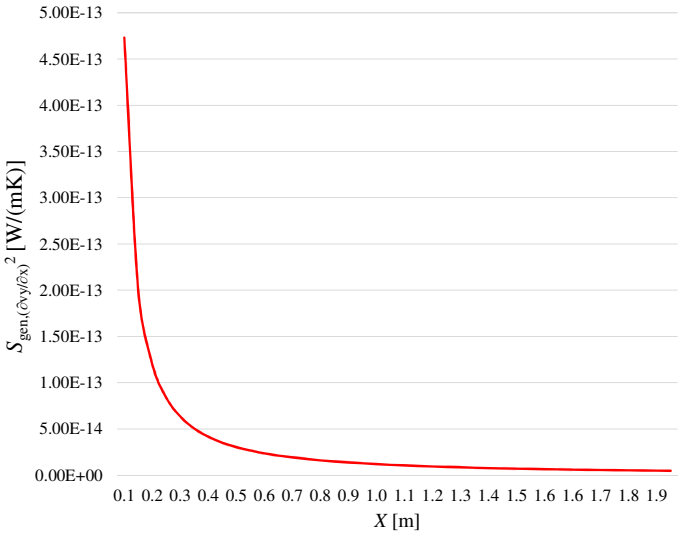

Figure 10. Dependence of entropy generation on wall height X and squared velocity gradient $(\partial v_y/\partial x)^2$ with $\eta_k = 282 \times 10^{-6}$ Pas, $\vartheta_s = 98.5$ °C and $\vartheta' = 100$ °C

Finally, the diagram in Figure 11 shows the entropy generation depending on the magnitude of X, the viscosity of the condensate and the product of the velocity gradient $2(\partial v_x/\partial y)\,(\partial v_y/\partial x)$. The result is similar in flow and values to the result given in Figure 8, which means that this part of the entropy generation can also be ignored.

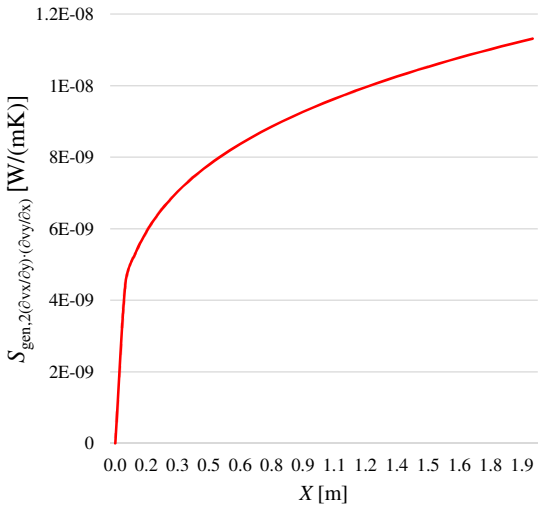

Figure 11. Dependence of entropy generation on wall height X and product of velocity gradients $2(\partial v_x/\partial y)\,(\partial v_y/\partial x)$ with $\eta_k = 282 \times 10^{-6}$ Pas, $\vartheta_s = 98.5$ °C and $\vartheta' = 100$ °C

Considering the viscosity and velocity gradients during laminar condensation of vapour, the total entropy production is obtained simply by summing the values shown in Figures 8-11. Of course, this total would be extremely small, only 10^{-7} W/mK, when it comes to the order of magnitude, so this total amount may be ignored with respect to the entropy generation deduced by means of eq. (16c).

Condensation of ammonia vapour

The second substance chosen to be completely condensed on a vertical flat wall with laminar condensate outflow is dry saturated vapour of pure ammonia with the saturation temperature ϑ' = 100 °C and the wall temperature of 98.5 °C (exactly the same as in the previous example). The saturation pressure was 62.553 bar and the following diagrams show some of the calculation results.

Henceforth, the diagram in Figure 12 shows the dependence on the flat wall height X, convective heat transfer coefficient and heat flow rate during the complete condensation of the ammonia vapour. The behaviour of these two values is similar to the one shown in Figure 1, except that in the latter case the values of convective heat transfer coefficient and heat flow rate are lower.

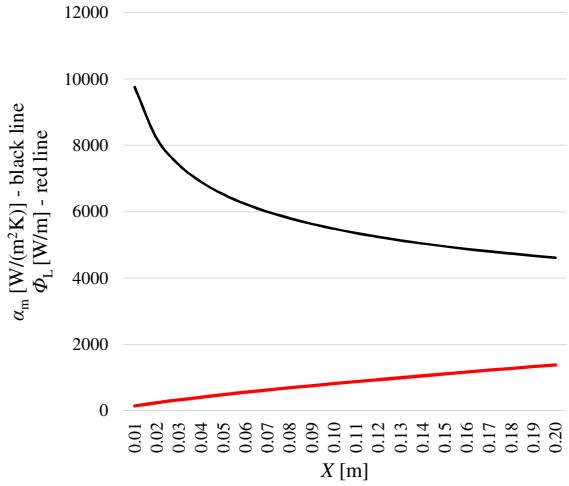

Figure 12. Dependence of heat transfer coefficient and heat flow rate on plane wall height X at condensation of saturated ammonia steam with ϑ' = 100 °C and ϑ_s = 98.5 °C

The diagram in Figure 13 shows the results of the calculation of the mass flow of the resulting condensate as well as its thickness, once again depending on the magnitude of X. It can be seen that in this case both values continuously grow with the increase in X, and in this case, too, only low values of thickness of the condensate film $\delta(x)$ and mass flow are produced.

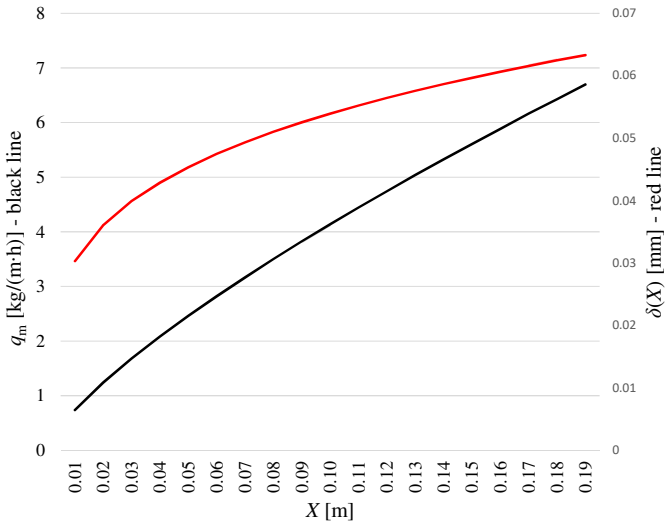

Figure 13. Dependence of condensate thickness and mass flow rate on wall height X for laminar ammonia condensate outflow with ϑ_s = 98.5 °C and ϑ' = 100 °C

Finally, the diagram in Figure 14 shows the entropy generation solely because of the existence of temperature gradients in the ammonia condensate stream, depending on the size of the variable *X*. The flow of these curves is similar to the flow of the curves given in Figure 7, with the difference being that lower condensation of ammonia vapour produces lower entropy generation values. The case of ammonia condensation also shows that the overall entropy generation is related exclusively to the temperature gradient $\partial T/\partial y$, as is the case with condensation of water vapour. This case also proves that the entropy generation resulting from the temperature gradient of $\partial T/\partial x$ has the order of magnitude amounting to 10^{-11} W/mK.

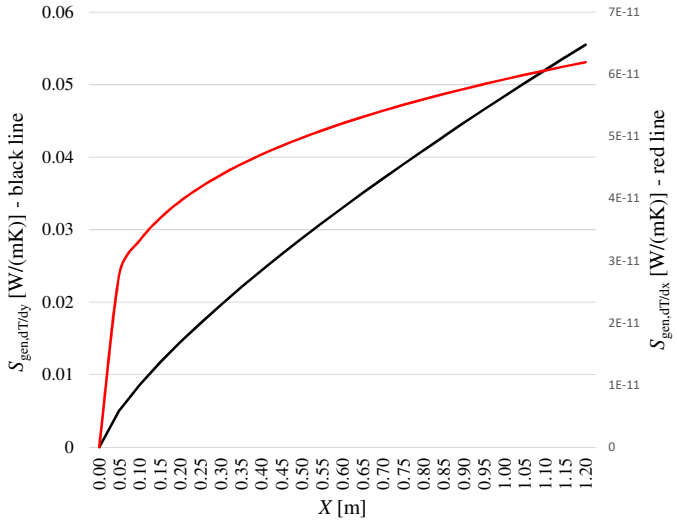

Figure 14. Dependence of entropy generation on wall height *X* and temperature gradients $\partial T/\partial y$ and $\partial T/\partial x$ in ammonia condensate with ϑ_s = 98.5 °C and ϑ' = 100 °C

The results of the calculation of the entropy generation resulting from the viscosity and the existence of velocity gradients have also proven to be imperceptible, almost equal to zero, so the results are not presented in this paper.

VERIFICATION OF THE CALCULATION USING A DIFFERENT METHOD

The previous analysis has shown that the entropy generation in its entirety is basically related only to the heat transfer in the *y*-axis, i.e., it occurs only because of the existence of the dominant temperature gradient $\partial T/\partial y$, and therefore the basic differential eq. (16c) makes it easier to derive the results in said case [28]:

$$\dot{S}_{gen} = \frac{T_A - T_B}{T_A T_B} \int \delta \Phi_{A,B} \tag{30}$$

with the fact that in eq. (30), object A represents a saturated vapour of temperature $T_A = T'$ and object B a wall of temperature $T_B = T_s$. The heat flow rate delivered by the saturated vapour to the wall, calculated by the meter of the width of the wall (b), is calculated according to the Bejan [25]:

$$\delta \Phi_{A,B} = \lambda_k \frac{T' - T_s}{\delta(x)} dx \tag{31}$$

Placing eq. (31) into eq. (30) with eq. (5) is equal to:

$$\dot{S}_{gen} = \lambda_k \frac{(T' - T_s)^2}{T_s T'} \int_0^X \frac{dx}{C x^{\frac{1}{4}}} = \frac{4}{3} \frac{(T' - T_s)^2}{T' T_s} \left[\frac{gr(\rho_k - \rho_p)\rho_k \lambda_k^3 X^3}{4\eta_k (T' - T_s)} \right]^{\frac{1}{4}} \tag{32}$$

Eq. (32) is identical to the result shown in the first addend of eq. (18). The equivalence of these two results confirms the fact that the dominant part of the entropy generation basically occurs at the molecular level related to the heat conduction through the condensate film.

CONCLUSIONS

The analysis that was carried out has shown that the laminar flow of the condensate is sustainable at relatively higher wall heights, at a small temperature difference $\vartheta' - \vartheta_s$ with regard to the restrictive criterion $Re_{\delta(x)} \leq 30$. In the example with water, where $\vartheta' - \vartheta_s = 100\ °C - 98.5\ °C = 1.5\ °C$, the height of the plane wall for laminar condensate outflow was 1.90 m. It was further shown that the resulting thicknesses of the condensate layer were very small and ranged from 0.0 to 0.09 mm. The obtained average values of the convective heat transfer coefficient decreased with increasing wall height X, and the obtained values have been markedly higher regarding the condensation of water vapour compared to the condensation of ammonia vapour, as shown quantitatively in Figure 1 and Figure 12.

With respect to the entropy generation, it must be emphasized that all the factors contributing to the entropy input, which were indicated in eq. (14), have been analytically derived. These factors include the entropy generation resulting from the heat conduction in the direction of the x and y coordinates, respectively, and they encompass the entropy generation resulting from the viscosity of the condensate and the existence of velocity gradients in the directions of the indicated axes. The obtained equations and their diagrammatic representation have shown that the dominant, in other words total entropy increase is directly related only to the heat conduction in the y-axis, or only related to the temperature gradient $\partial T/\partial y$, where the y-axis corresponds to the thickness of the condensate. This means that the total entropy production is actually determined by eq. (16c), i.e., eq. (32), and it can be seen from the diagrams in Figure 7 and Figure 14 that these values increase with the increase of plane wall height X.

The inputs of the other factors, explicitly given by eq. (17c), and eq. (26-29) and the corresponding diagrammatic representations in Figures (7-11) and Figure 13, have shown that their input to the total amount of entropy generation was little short of zero. It is evident that there were obtained values of the entropy generation from 10^{-12} to 10^{-7} W/mK, but at the same time it has also been concluded that the contribution of the biggest gradient $\partial v_x/\partial y$, although also imperceptible in relation to the total entropy production, is 10^5 higher in comparison to other velocity gradients.

NOMENCLATURE

b	wall width	[m]
q_m	mass flow rate of condensate	[kg/s]
r	specific latent heat	[J/kg]
S_{cond}	entropy production as a result of heat conduction	[W/m^{3}K]
S_{dis}	entropy production as a result of dissipation of mechanical energy	[W/m^{3}K]
$\dot{S}_{gen}$	entropy generation	[W/mK]
$\dot{S}_{gen,dT/dy}$	entropy generation due to existence of temperature gradient in y-axis directions	[W/mK]
$\dot{S}_{gen,dT/dx}$	entropy generation due to existence of temperature gradient in x-axis directions	[W/mK]
$\dot{S}_{gen,cond}$	entropy generation due to existence of temperature gradients, in both y-axis and x-axis directions	[W/mK]

$\dot{S}_{gen,[(\partial v_x/\partial x)^2+(\partial v_y/\partial y)^2]}$	entropy generation due to η_k and value $(\partial v_x/\partial x)^2 + (\partial v_y/\partial y)^2$	[W/mK]
$\dot{S}_{gen,(\partial v_x/\partial y)^2}$	entropy generation due to η_k and value $(\partial v_x/\partial y)^2$	[W/mK]
$\dot{S}_{gen,(\partial v_y/\partial x)^2}$	entropy generation due to η_k and value $(\partial v_y/\partial x)^2$	[W/mK]
$\dot{S}_{gen,2(\partial v_y/\partial x)\,(\partial v_x/\partial y)}$	entropy generation due to η_k and value $2(\partial v_y/\partial x)\,(\partial v_x/\partial y)$	[W/mK]
T_A	object A temperature	[K]
T_B	object B temperature	[K]
T'	saturation temperature	[K]
T_s	wall temperature	[K]
v_x	velocity in the direction of the x-axis	[m/s]
$\bar{v}_X$	average velocity in the direction of the x-axis	[m/s]
v_y	velocity in the direction of the y-axis	[m/s]
X	wall height	[m]
$\frac{\partial T}{\partial x}$	temperature gradient in x-axis directions	[K/m]
$\frac{\partial T}{\partial y}$	temperature gradient in y-axis directions	[K/m]
Greek letters		
α_m	average convective heat transfer coefficient	[W/m^{2}K]
$\delta(x)$	thickness of the condensate layer	[m]
η_k	dynamic viscosity of condensate	[Pa s]
λ_k	thermal conductivity of the condensate	[W/mK]
ρ_k	condensate density	[kg/m^3]
ρ_p	steam density	[kg/m^3]
Φ_L	heat flow rate	[W/m]

REFERENCES

1. Nusselt, W. A., The Surface Condensation of Water Vapor, in: *Journal of the Association of German Engineers* (in German), Vol. 60, pp 541-546, 1916.
2. Hygum, M. A., Karlin, I. V. and Popok, V. N., Free Surface Entropic Lattice Boltzmann Simulations of Film Condensation on Vertical Hydrophilic Plates, *International Journal of Heat and Mass Transfer*, Vol. 87, pp 576-582, 2015, https://doi.org/10.1016/j.ijheatmasstransfer.2015.04.032
3. Li, G. C. and Yang, S. A., Entropy Generation Minimization of Free Convection Film Condensation on an Elliptical Cylinder, *International Journal of Thermal Sciences*, Vol. 46, No. 4, pp 407-412, 2007, https://doi.org/10.1016/j.ijthermalsci.2006.06.007
4. Wu, J., Sun, X., Li, X. and Liu, Y., Research on Film Condensation Heat Transfer at the Inside of Spiral Coil Tube, *International Journal of Heat and Mass Transfer*, Vol. 147, 2020, https://doi.org/10.1016/j.ijheatmasstransfer.2019.118891
5. Wu, J., Wang, L. and Liu, Y., Research on Film Condensation Heat Transfer of the Shell Side of the Spiral Coil Heat Exchanger, *International Journal of Heat and Mass Transfer*, Vol. 125, pp 1349-1355, 2018, https://doi.org/10.1016/j.ijheatmasstransfer.2018.05.029
6. Charef, A., Feddaoui, M., Najim, M. and Meftah, H., Liquid Film Condensation from Water Vapour Downward Along a Vertical Tube, *Desalination*, Vol. 409, pp 21-31, 2017, https://doi.org/10.1016/j.desal.2017.01.018
7. Lee, H. and Son, G., Level-Set Based Numerical Simulation of Film Condensation in a Vertical Downward Channel Flow, *International Communications in Heat and Mass Transfer*, Vol. 95, pp 171-181, 2018, https://doi.org/10.1016/j.icheatmasstransfer.2018.05.001

8. Pati, S., Som, S. K. and Chakraborty, S., Slip-Driven Alteration in Film Condensation over Vertical Surfaces, *International Communications in Heat and Mass Transfer*, Vol. 46, pp 37-41, 2013, https://doi.org/10.1016/j.icheatmasstransfer.2013.05.002
9. Ali, M., Rad, M. M., Nuhait, A., Almuzaiqer, R., Alimoradi, A. and Tlili, I., New Equations for Nusselt Number and Friction Factor of the Annulus Side of the Conically Coiled Tubes in Tube Heat Exchangers, *Applied Thermal Engineering*, Vol. 164, 2020, https://doi.org/10.1016/j.applthermaleng.2019.114545
10. Yang, S. A., Li, G. C. and Yang, W. J., Thermodynamic Optimization of Free Convection Film Condensation on a Horizontal Elliptical Tube with Variable Wall Temperature, *International Journal of Heat and Mass Transfer*, Vol. 50, No. 23-24, pp 4607-4613, 2007, https://doi.org/10.1016/j.ijheatmasstransfer.2007.03.019
11. Qu, Z. G., Li, A. and Tao, W. Q., Numerical Study of Film Condensation on a Metallic Foam-Sintered Plate with Considering Convection and Super-Cooling Effects, *International Communications in Heat and Mass Transfer*, Vol. 79, pp 105-113, 2016, https://doi.org/10.1016/j.icheatmasstransfer.2016.10.006
12. Wu, J., Tian, Q., Sun, X., Zhao, J., Wang, L., Peng, X. and Liao X., Numerical Simulation and Experimental Research on the Comprehensive Performance of the Shell Side of the Spiral Wound Heat Exchanger, *Applied Thermal Engineering*, Vol. 163, 2019, https://doi.org/10.1016/j.applthermaleng.2019.114381
13. Ahn, T., Kang, J., Bae, B., Jeong, J. J. and Yun, B., Steam Condensation in Horizontal and Inclined Tubes under Stratified Flow Conditions, *International Journal of Heat and Mass Transfer*, Vol. 141, pp 71-87, 2019, https://doi.org/10.1016/j.ijheatmasstransfer.2019.06.056
14. Rajkumar, M. R., Praveen, A. and Krishnan, R. A., Experimental Study of Condensation Heat Transfer on Hydrophobic Vertical Tube, *International Journal of Heat and Mass Transfer*, Vol. 120, pp 305-315, 2018, https://doi.org/10.1016/j.ijheatmasstransfer.2017.12.019
15. Yan, D., Gu, M. and Zou, L., Numerical Analysis of the Heat Transfer in a Naphthalene Heat Pipe Based on the Modified Nusselt Model, *Applied Thermal Engineering*, Vol. 167, 2020, https://doi.org/10.1016/j.applthermaleng.2019.114730
16. Dung, S. C. and Yang, S. A., Second Law Based Optimization of Free Convection Film-Wise Condensation on a Horizontal Tube, *International Communications in Heat and Mass Transfer*, Vol. 33, No. 5, pp 636-644, 2006, https://doi.org/10.1016/j.icheatmasstransfer.2006.01.013
17. Esfahani, J. A. and Modirkhazeni, M., Entropy Generation of Forced Convection Film Condensation on a Horizontal Elliptical Tube, *Comptes Rendus Mécanique*, Vol. 340, No. 7, pp 543-551, 2012, https://doi.org/10.1016/j.crme.2012.03.008
18. Ding, H., Li, Y., Lakzian, E., Wen, C. and Wang, C., Entropy Generation and Exergy Destruction in Condensing Steam Flow Through Turbine Blade with Surface Roughness, *Energy Conversion and Management*, Vol. 196, pp 1089-1104, 2019, https://doi.org/10.1016/j.enconman.2019.06.066
19. Sheikholeslami, M., Darzi, M. and Li, Z., Experimental Investigation for Entropy Generation and Exergy Loss of Nano-Refrigerant Condensation Process, *International Journal of Heat and Mass Transfer*, Vol. 125, pp 1087-1095, 2018, https://doi.org/10.1016/j.ijheatmasstransfer.2018.04.155
20. Aghakhani, A., Pordanjani, A. H., Afrand, M., Sharifpur, M. and Meyer, J. P., Natural Convective Heat Transfer and Entropy Generation of Alumina/Water Nanofluid in a Tilted Enclosure with an Elliptic Constant Temperature: Applying Magnetic Field and Radiation Effects, *International Journal of Mechanical Sciences*, Vol. 174, 2020, https://doi.org/10.1016/j.ijmecsci.2020.105470
21. Gholamalipour, P., Siavashi, M. and Doranehgard, M. H., Eccentricity Effects of Heat Source Inside a Porous Annulus on the Natural Convection Heat Transfer and Entropy

Generation of Cu-Water Nanofluid, *International Communications in Heat and Mass Transfer*, Vol. 109, 2019, https://doi.org/10.1016/j.icheatmasstransfer.2019.104367
22. Rashidi, S., Akarm, S., Bovand, M. and Ellahi, R., Volume of Fluid Model to Simulate the Nanofluid Flow and Entropy Generation in a Single Slope Solar Still, *Renewable Energy*, Vol. 115, pp 400-410, 2018, https://doi.org/10.1016/j.renene.2017.08.059
23. Aliabadi, M. A. F., Jahangiri, A., Khazaee, I. and Lakzian, E., Investigating the Effect of Water Nano-Droplets Injection Into the Convergent-Divergent Nozzle Inlet on the Wet Steam Flow Using Entropy Generation Analysis, *International Journal of Thermal Sciences*, Vol. 149, 2020, https://doi.org/10.1016/j.ijthermalsci.2019.106181
24. Vatanmakan, M., Lakzian, E. and Mahpeykar, M. R., Investigating the Entropy Generation in Condensing Steam Flow in Turbine Blades with Volumetric Heating, *Energy*, Vol. 147, pp 701-714, 2018, https://doi.org/10.1016/j.energy.2018.01.097
25. Bejan, A., *Entropy Minimisation Optimisation*, CRC Press, Boca Raton, Florida, USA, 2000.
26. Hamiche, A. M., Stambouli, A. B. and Flazi, S., A Review of the Water-Energy Nexus, *Renewable and Sustainable Energy Reviews*, Vol. 65, pp 319-331, 2016, https://doi.org/10.1016/j.rser.2016.07.020
27. Cengel, Y. A., *Heat Transfer, A Practical Approuch*, McGraw-Hill, Boston, Massachusetts, USA, 2003.
28. Bošnjaković, F. and Knoche, K. F., *Technical Thermodynamic* (7th completely revised and expanded edition) (in German), Steinkopff Darmstadt, Darmstadt, Germany, 1988.

Paper submitted: 26.12.2019
Paper revised: 14.03.2020
Paper accepted: 30.03.2020